A Prestressed Cable Network Model of the Adherent Cell Cytoskeleton

Mark F. Coughlin* and Dimitrije Stamenović†
*Department of Bioengineering, University of California, San Diego, La Jolla, California 92093 and †Department of Biomedical Engineering, Boston University, Boston, Massachusetts 02215 USA

ABSTRACT A prestressed cable network is used to model the deformability of the adherent cell actin cytoskeleton. The overall and microstructural model geometries and cable mechanical properties were assigned values based on observations from living cells and mechanical measurements on isolated actin filaments, respectively. The models were deformed to mimic cell poking (CP), magnetic twisting cytometry (MTC) and magnetic bead microrheometry (MBM) measurements on living adherent cells. The models qualitatively and quantitatively captured the fibroblast cell response to the deformation imposed by CP while exhibiting only some qualitative features of the cell response to MTC and MBM. The model for CP revealed that the tensed peripheral actin filaments provide the key resistance to indentation. The actin filament tension that provides mechanical integrity to the network was estimated at ~158 pN, and the nonlinear mechanical response during CP originates from filament kinematics. The MTC and MBM simulations revealed that the model is incomplete, however, these simulations show cable tension as a key determinant of the model response.

INTRODUCTION

Many biological functions of adherent cells are partly regulated through cell shape and deformability (Folkman and Mascona, 1978; Elson, 1988; Singhvi et al., 1994; Chen et al., 1997; Chicurel et al., 1998; Janmey, 1998). A growing body of evidence indicates that the primary control of adherent cell shape and deformability is exerted at the level of the cytoskeletal (CSK) filaments. For example, cell shape is determined by both internal structures dense in CSK filaments (e.g., pseudopodia) and transmembrane linkages connecting CSK filaments and extracellular matrix proteins (e.g., at focal adhesion complexes). Moreover, cell deformability assessed by mechanical measurement is largely determined by the composition, architecture, and force in the underlying CSK filaments. In particular, an interconnected network of actin filaments provides the main force-bearing CSK structure within anchorage dependent cells. A complete description of CSK filament function in the cell remains elusive. To understand how physical forces regulate biological function, the microstructural mechanisms by which the CSK filaments give rise to macroscopic cellular properties must be addressed.

An engineering approach to CSK mechanics has provided new tools to address the mechanisms by which cells resist deformation (Stamenović and Wang, 2000). We recently used a conceptual cable network model to connect microstructrual CSK parameters to macroscopic properties of adherent cells (Stamenović and Coughlin, 1999). The actin CSK was depicted as a network of randomly oriented tension-supporting cables. A key feature of the model was that actin filaments supported a prestress, i.e., a preexisting tensile stress provided either by the cell contractile apparatus or cell distension on the substrate. Transparent mathematical expressions related CSK prestress and elastic modulus to microstructural parameters characterizing CSK forces and architecture. A merit of the prestressed cable network as a model of CSK mechanics is that some details of the CSK microstructure need not be explicitly specified. However, this generality also limits the model's predictive capacity. For example, an expression for the cell elastic modulus was obtained without designating the nature of the cable interconnections, but the strongest prediction was then a lower bound. To obtain more definite predictions of the CSK forces and elastic properties requires additional intricacies of the CSK microstructure to be postulated. Previously, interconnected elastic cable networks with cables represented by linear elastic springs provided quantitative predictions of erythrocyte elastic properties (Hansen et al., 1996) and remarkable correspondence to the erythrocyte CSK response in micropipette aspiration experiments (Discher et al., 1998). However, it is not clear that cable network models that describe the mechanics of suspended cells are as appropriate for anchorage dependent cells. The purpose of this investigation was to examine the possibility that cable networks can qualitatively and quantitatively predict the mechanical response of anchorage dependent cells subjected to various mechanical perturbations.

In the current study, two prestressed cable networks were examined as models of the adherent cell actin CSK. In one model, the cables were organized into a planar lattice of regular hexagons, and in the other, the cables were organized into a planar lattice of equilateral triangles. The geometric parameters and cable elastic properties were assigned based on data from the literature. The models were deformed to mimic cell poking (CP), magnetic twisting cytometry (MTC), and magnetic bead microrheometry (MBM) measurements on living adherent cells. The predicted responses

Submitted May 23, 2002, and accepted for publication October 7, 2002.
Address reprint requests to Mark F. Coughlin, Physiology Dept., Harvard School of Public Health, 665 Huntington Avenue, Boston, Massachusetts 02115. Tel.: 617-432-2610; E-mail: mcoughli@hsph.harvard.edu.

0006-3495/03/02/1328/09 $2.00

were compared to published data. The models were used to identify mechanisms that underlie CSK deformability and to predict CSK forces and elastic properties.

MODEL FORMULATIONS

The adherent cell CSK was modeled as a network of elastic cables interconnected by frictionless pin-joints. Two microstructural geometries were considered. In the first model, three cables emanate from each pin-joint as the cables enclose an array of hexagons (Fig. 1 *A*). In the second model, six cables emanate from each pin-joint as the cables form an array of triangles (Fig. 1 *B*). The main difference between the two models is the number of constraints on the pin-joint degrees of freedom. Each cable emanating from a pin-joint represents a constraint on its position. Because more cables attach to each pin-joint in the triangular network, it is necessarily more constrained than the hexagonal network. In both models, the position of the outermost pin-joints (attachments) was fixed such that the hexagons or triangles in the initial (undeformed) model configuration were identical in size and shape and arranged into concentric rings (Fig. 1). The microstructural geometry of each model is characterized by the cable length in the initial configuration (l_0; Fig. 1, *insets*). The overall model size is characterized by the model projected area (S), defined as the area inside the attachments. The relationship between S, the number of concentric rings N and l_0 in the case of the hexagonal network is given by

$$S = \frac{\sqrt{3}}{2}(1 + 3N)^2 l_0^2, \tag{1}$$

or in the case of the triangular network by

$$S = \frac{3\sqrt{3}}{2}(1 + N)^2 l_0^2. \tag{2}$$

Because the cable elements in the network represent actin filaments in the CSK, the cable mechanical behavior was based on observations from individual actin filaments. First, actin filaments respond to small extensions like stiff linear springs (Kojima et al., 1994). Second, the actin filament bending stiffness is small (Gittes et al., 1993), and their lateral dimension is typically much smaller than their length. This suggests that individual actin filaments cannot support substantial compressive loads without collapsing (buckling). Thus, the cables were assumed to be linearly elastic (Hookean) and support only tensile forces. The cable force-extension relationship is given by

$$F = \begin{cases} E_c A_c (l/l_r - 1) & \text{if } l > l_r \\ 0 & \text{if } l \le l_r \end{cases}, \tag{3}$$

where F is the cable force, E_c is the cable elastic (Young's) modulus, A_c is the cable cross-sectional area, l is the cable deformed length and l_r is the cable resting length.

The five model parameters: l_0, S, E_c, A_c and l_r were assigned values based on data in the literature. Because there is no direct observation of l_0 in living cells, l_0 was estimated from an effective CSK pore size (D_p) in adherent cells. Experimental observations of the actin CSK in adherent endothelial and fibroblast cells reveal a network with $D_p \approx 50$–200 nm (Luby-Phelps et al., 1986; Amos and Amos, 1991; Janmey, 1996; Satcher et al., 1997; Caille et al., 1998). In this study, calculations were performed with the intermediate value $D_p = 100$ nm. It was assumed that each hexagon and triangle enclosed a pore with diameter $D_p = \sqrt{3}l_0$ and $\sqrt{3}l_0/3$, respectively (Fig. 1, *insets*) in the initial configuration. It follows that $l_0 = 57.7$ and 173.2 nm for the hexagonal and triangular networks, respectively. The model area S was chosen to match to two representative measurements of endothelial cell projected area of 350 and 1640 μm^2, corresponding to round and spread cells (Wang and Ingber, 1994). It follows from Eqs. 1 and 2 and $D_p = 100$ nm that $N = 116$ and 251 for round and spread cells in the hexagonal network model, respectively, and $N = 66$ and 144 round and spread cells in the triangular network, respectively. The cable properties were determined from published values of the Young's modulus $E_c = 2.8$ GPa and cross-sectional area $A_c = 18.8$ nm^2 of individual actin filaments (Gittes et al., 1993). The final free model parameter l_r is determined by specifying the cable force in the initial configuration F_0 using Eq. 3, $l_r = l_0 E_c A_c/(F_0 + E_c A_c)$. Only F_0 between 0 and the highest measured yield force for individual actin filaments of $F_{MAX} \approx 600$ pN (Tsuda et al., 1996) were examined.

The position of the pin-joints inside the attachments was determined by equilibrium equations. A Cartesian coordinate system $OXYZ$ was placed at the center of the model with the Z-axis normal to the plane of the network. A pin-joint was in equilibrium when the cable forces exerted on the joint were balanced. Force balance in the X-direction for a pin-joint with coordinates (x_0, y_0, z_0) and n_c cables terminating at pin-joints with coordinates (x_i, y_i, z_i), $i = 1, \ldots, n_c$, is given by

$$\sum_{i=1}^{n_c} \frac{F_i (x_i - x_0)}{L_i} = 0, \tag{4}$$

where F_i is the force in the cable, $L_i = \sqrt{(x_i - x_0)^2 + (y_i - y_0)^2 + (z_i - z_0)^2}$ is the length of the cable spanning the joints at (x_0, y_0, z_0) and (x_i, y_i,

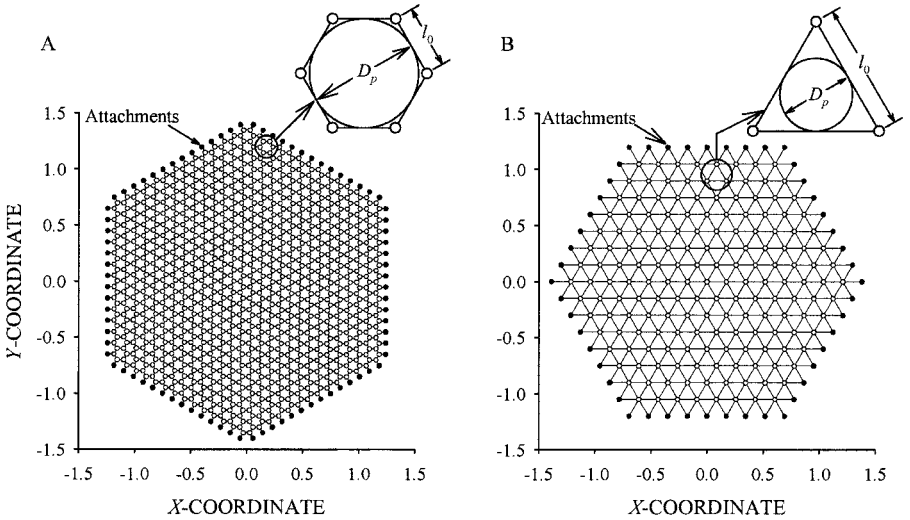

FIGURE 1 (*A*) Hexagonal and (*B*) triangluar cable network models for the adherent cell cytoskeleton. The networks are composed of elastic cables (*lines*) interconnected by pin-joints (*circles*) into an array with $N = 14$ and 7 concentric rings of hexagons and triangles, respectively. The attachments (*solid circles*) are pin-joints fixed to the rigid substratum. (*Insets*) An individual hexagon and triangle from the undeformed networks. Each hexagon and triangle encompasses a pore of diameter D_p with cable length of l_0.

z_i), and $n_c = 3$ and 6 for the hexagonal and triangular networks, respectively. Equations for force balance in the Y- and Z-directions are obtained from Eq. 4 by interchanging the X-coordinates with Y- and Z-coordinates, respectively.

Model equilibrium was established by iteratively solving the equilibrium equations (Eq. 4) for each pin-joint (except the attachments) until all equilibrium equations were simultaneously satisfied. The criteria dictating pin-joint equilibrium was a net force less than 10^{-6} pN in each coordinate direction. The coordinates of pin-joints not satisfying the equilibrium criteria were adjusted using a Newton-Raphson method (Gerald and Wheatley, 1989). All computations were performed on the Power Challenge Array facility of the Boston University Scientific Computation and Visualization Center.

MODEL IMPLEMENTATION

The models were deformed to mimic CP, MTC, and MBM measurements on adherent cells. A brief description of each measurement technique and its implementation in the model is described next.

Cell poking

The CP measurement technique has been used to assess the mechanical properties of various adherent cells (McConnaughey and Petersen, 1980; Petersen et al., 1981; Petersen et al., 1982; Elson et al., 1983; Zahalak et al., 1990). In studies of fibroblast cell deformability (Petersen et al., 1982; Elson et al., 1983; Cai et al., 1998), a cylindrical 2 μm-diameter glass stylus indented the cell surface. The relationship between the stylus indentation depth and force revealed primarily the subcortical CSK network mechanical properties (Petersen et al., 1981; Petersen et al., 1982). An important feature of the CP technique is that the stylus does not directly bind to CSK components or associated proteins.

To simulate the CP technique in the cable network model, the stylus was idealized as a frictionless, rigid circular cylinder (punch) with diameter $d = 2$ μm. The stylus was applied at the center of the model. The indentation of the stylus (u) on adherent cells was mimicked in the model by imposing the following constraints on the positions of the pin-joints: (1) the vertical Z-coordinates of the pin-joints under the punch were such that $z \leq -u$ and (2) the X- and Y-coordinates of the pin-joints located outside the punch diameter were not allowed to penetrate the side of the punch, $x^2 + y^2 > (D/2)^2$ when $z > -u$. Similarly, cables were not allowed to penetrate the surface of the punch. Cables connecting pin-joints under and outside the punch were stretched over the edge of the punch through an intermediate point with coordinates (x_p, y_p, u) (Fig. 2 *A*). The coordinates of the intermediate point were found such that the net circumferential force due to the cable segments under and outside the punch were balanced. The position of all the pin-joints was determined by Eq. 4. It was sufficient to compute the equilibrium positions for only one-twelfth of all pin-joints because of model symmetry.

In the deformed model configuration, the indentation force W was computed from the equilibrium equation of the punch (Fig. 2 *B*). The equation for force balance between the Z-component of the cable forces exerted on the punch and W is given by

$$W + \sum_{i=1}^{C} \frac{F_i(z_i - u)}{l_i} = 0, \qquad (5)$$

where F_i is the cable force, $l_i = \sqrt{(x_i - x_p)^2 + (y_i - y_p)^2 + (z_i - u)^2}$ is the distance between the pin-joint with coordinates (x_i, y_i, z_i) located outside the punch and the point with coordinates (x_p, y_p, u) on the edge of the punch, and C is the number of cables crossing the edge of the punch. The X- and Y-components of the cable forces exerted on the punch balance by model symmetry. The relationship between u and W was compared to data obtained from CP measurements during the indentation of adherent fibroblast cells.

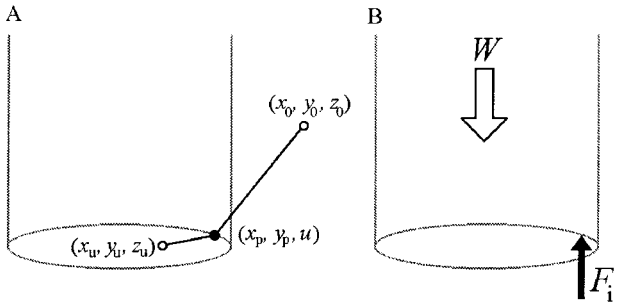

FIGURE 2 (*A*) Schematic diagram of a single cable stretched over the edge of the punch in the model for cell poking. A pin-joint located under the face of the punch connects a pin-joint located outside the diameter of the punch. Because the punch is rigid, the cable stretches through the point with coordinates (x_p, y_p, u) on the edge of the punch. (*B*) A free-body diagram of the punch. The cable stretched over the edge of the punch exerts a force F_i on the punch that partly balances the indentation force W. The total force exerted by the network on the punch is the sum of all F_i from cables crossing the edge of the punch.

Magnetic twisting cytometry

The MTC measurement technique has been used to assess the mechanical properties of various adherent cells (Wang et al., 1993; Wang and Ingber, 1994; Hubmayr et al., 1996; Cai et al., 1998). In studies of endothelial cell deformability, ligand coated magnetic beads with 1.4 or 5.5 μm diameter were bound to the cells via integrin surface receptors (Wang et al., 1993; Wang and Ingber, 1994). The attached beads were polarized, and an applied magnetic field induced a magnetic moment causing bead rotation. The relationship between the bead rotation and magnetic moment was used to assess the cellular mechanical properties. An important feature of the MTC technique is the interaction between the bead and CSK. The intracellular domain of the bead bound integrin receptors accumulate focal adhesion proteins and interact with the CSK (Wang et al., 1993). As a consequence, the main intracellular structures probed by MTC are both the cortical CSK network and possibly filaments deeper within the cytoplasm.

To implement the MTC technique in the cable network model, the cell bound magnetic beads were idealized as rigid spheres. It was assumed that one bead was bound to the model; it was half embedded in the network and centered within the attachments in the undeformed configuration. Although the bead was considered rigid for bead rotation, the pin-joints and cables in the undeformed configuration were allowed to freely penetrate the bead surface (Fig. 3). This simplified scheme for the interaction of the bead and network allowed the initial network configuration to be planar and regular. If the network interacted with the bead surface, then an initial force would be required to embed the bead in the network and the regular network geometry would be distorted in the initial configuration. The pin-joints falling within the bead boundary (bound pin-joints) were distinguished from those outside the bead boundary (free pin-joints). The rotation of a surface bound magnetic bead was mimicked in the model by collectively rotating the bound pin-joints as a rigid body through an angle θ about the Z-axis through the bead center. The equilibrium positions of the free pin-joints were determined from Eq. 4. Thus, the positions of the bound pin-joints were prescribed whereas the positions of the free pin-joints were computed.

In the deformed configuration, the cables connecting free and bound pin-joints exert a moment on the bead. The moment was computed from the bead equilibrium equations. For a bound pin-joint located at (x_i, y_i) connected by

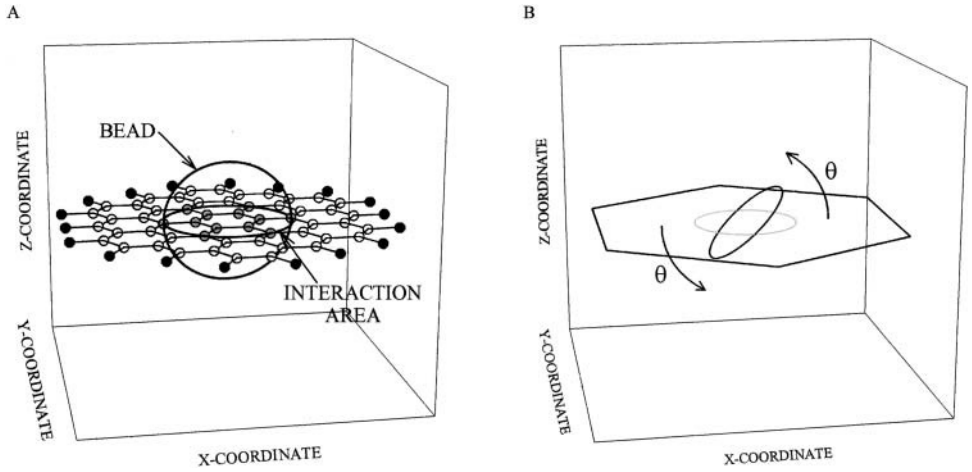

FIGURE 3 Oblique views of a hexagonal network with $N = 3$ and an attached bead. The gray circles are fixed pin-joints located where the bead intersects the network, open circles are the free pin-joints, and black circles are attachments.

a cable to a free pin-joint, the equation for moment balance in the Z-direction (M_Z) about origin of the coordinate system is given by

$$M_Z + \sum_{i=1}^{C}(x_i F_Y - y_i F_X) = 0, \tag{6}$$

where C is the number of cables connecting fixed and bound pin-joints, and F_X and F_Y are the X- and Y-components of the force in the i^{th} cable. Force balance equations are satisfied by model symmetry. The relationship between M_Z and bead rotation were interpreted as described for MTC measurements (Wang and Ingber, 1994); shear stress σ was defined as the moment per bead volume $\sigma = M_Z/V$, and θ was regarded as a shear strain. It was sufficient to compute the equilibrium positions for only one-twelfth of the free pin-joints because of model symmetry.

Magnetic bead microrheometry

Magnetic bead microrheometry (MBM) has been used to study the mechanics of adherent endothelial and fibroblast cells (Bausch et al., 1998; Bausch et al., 2001). The MBM technique has similarities to MTC. Magnetic beads with 4.5 μm-diameter were bound to integrin receptors on the cell surface and polarized in a magnetic field. A strong gradient in magnetic field induced a pulling force in each bead causing bead displacement. The relationship between the bead displacement and pulling force revealed the CSK mechanical properties. As noted for MTC, the surface bound beads connect to the CSK through a collection of accessory proteins.

To implement MBM in the network model, the bead was modeled as a rigid sphere with frictionless, impenetrable surface. It was assumed that a single bead was bound to the network, the bead was centered within the attachments, and half the bead was embedded in the network as described for MTC. To mimic the pulling of an attached magnetic bead, the bound pin-joints were displaced as a rigid body in the XY-plane by an amount δ. Thus, the positions of the bound pin-joints in the deformed configuration were prescribed, and the positions of the free pin-joints in the deformed configuration were determined by Eq. 4.

In the equilibrium configuration, the network exerts a force on the bead in two ways. The first force is due to the cables connecting bound and free pin-joints that stretch as a result of δ and exert a pulling force on the displaced bead. A second force arises from free pin-joints that accumulate on the bead surface as a result of δ. Because the bead is impenetrable, those free pin-joints will exert a pushing force on the bead. The net force on the bead $\mathcal{F}$ was the sum of the pushing and pulling forces in the direction of δ. For a bead in the deformed configuration, the component of $\mathcal{F}$ in the X-direction ($\mathcal{F}_X$) was given by

$$\mathcal{F}_X = \sum_{i=1}^{C} \frac{F_i(x_i^f - x_i^b)}{L_i} + \sum_{i=1}^{P} T_i, \tag{7}$$

where F_i is the force in the cable connecting the free and bound pin-joints with coordinates (x_i^f, y_i^f, z_i^f) and (x_i^b, y_i^b, z_i^b), respectively, L_i is the cable length, T_i is the pushing force exerted by pin-joint i on the bead, C is the number of cables connecting free and bound pin-joints, and P is the number of pin-joints exerting a pushing force on the bead. It was sufficient to consider only half the model to determine the equilibrium positions of the free pin-joints.

RESULTS

Cell poking

For both the hexagonal (Fig. 4) and triangular (Fig. 5) networks in the round and spread configurations, W increases nonlinearly with increasing u. The slope of the u vs. W relationship, which indicates model rigidity, increases with u. This particular nonlinearity is exhibited by fibroblast cells during CP measurements (Petersen et al., 1982; Elson et al., 1983). For a given u, W increased with increasing F_0 in both models. That is, resistance to indentation increased with increasing F_0. This trend is consistent with the observed increase in stiffness in fibroblast cells containing constitutively active myosin light chain kinase (Cai et al., 1998), which is thought to increase actin filament tension. The quantitative predictions of W from both models in the spread configuration are in excellent agreement with experimental data from the literature (Fig. 4 A and Fig. 5 A). The measured W falls between the predicted upper and lower bounds for all u and $u < 2.0$ μm in the hexagonal and triangular models, respectively. There is also good quantitative correspondence from the round configuration but over a narrower range of u than was found in the spread configuration (Fig. 4 B and Fig. 5 B). The measured data fall within the predicted upper and lower bounds for $u \leq \sim 1.2$ and ~ 0.7 μm in the hexagonal and triangular models, respectively.

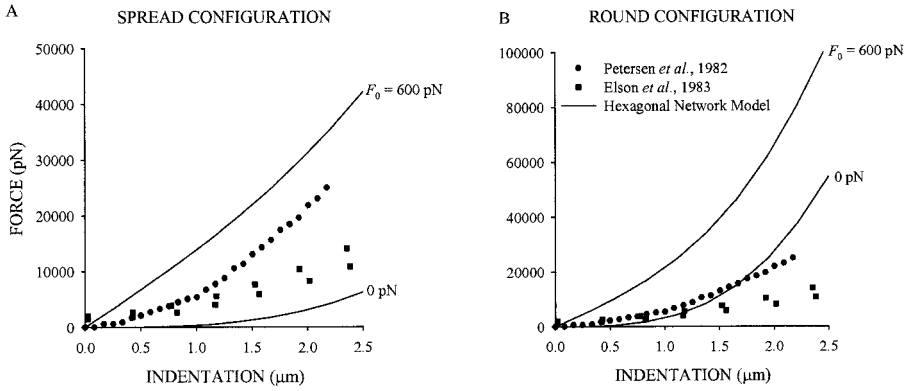

FIGURE 4 Hexagonal cable network model response to cell poking deformation. Comparison of the predicted indentation u versus force W relationships (*lines*) and measured data (*symbols*) from Petersen et al. (1982) and Elson et al. (1983) for the (*A*) spread and (*B*) round model configurations with $F_0 = 0$ and 600 pN.

For both the hexagonal and triangular networks in the spread configuration with $F_0 = 0$, the peak and the width of the cable force distribution increase with increasing u (Fig. 6). Thus, the force carried by most cables increases with indentation. The cable force distributions in the two models show important differences. The force in each cable in the hexagonal network increases with increasing u, and no cable reaches its resting length (Fig. 6 *A*). At the maximum indentation $u = 2.5$ μm, all the cables carry a substantial force $F > 102$ pN. Thus, even peripheral cables contribute to resistance to a localized deformation as forces are transmitted throughout the network. In the triangular network, some cables carry forces that far exceed the maximum force in the corresponding hexagonal network, and some cables carry little force even for $u = 2.5$ μm (Fig. 6 *B*). These observations show that while the force resisting indentation is transmitted throughout both networks, many cables carry very little force in the more constrained triangular network. In both models, the shape of the cable force distribution remained unchanged during deformation. Similar trends were found for $F_0 = 600$ pN and the round configuration.

The close qualitative and quantitative correspondence between the predicted u vs. W relationship and the measured cell response has several implications. First, it suggests that the initial resistance to indentations of adherent fibroblast cells is provided by the cortical actin filaments organized as an interconnected elastic cable network. Second, the nonlinear W vs. u curves exhibited by cells in response to CP may arise from filament kinematics and not an intrinsic nonlinear filament property. Third, F_0 is a key determinant of adherent fibroblast cell deformability.

Magnetic twisting cytometry

In both the hexagonal and triangular networks, in the round and spread configurations, shear stress σ increases nonlinearly with increasing θ (Fig. 7 *A*). This strain hardening is consistent with MTC measurements on adherent endothelial cells (Wang et al., 1993; Wang and Ingber, 1994). For a given θ, σ increases with increasing F_0 in both models. This is consistent with the observed increase in endothelial cell rigidity after mechanical (Pourati et al., 1998) and pharmacological (Cai et al., 1998) increases in CSK tensile forces. The quantitative predictions of σ from all models exceed the measured values by several orders of magnitude (Fig. 7 *B*). Moreover, the model is more deformable in the spread than round configuration and predicts an increase in deformability with increasing bead size (Coughlin, 2000). Both these trends are opposite to the observed behavior (Wang and Ingber, 1994).

The model qualitatively predicts some observed responses to MTC, however, other trends are opposite to the observed behavior and the quantitative predictions are exceedingly high. This suggests that the model is incomplete. The overprediction of cell deformability even with $F_0 = 0$ suggests that the mechanisms determining the model

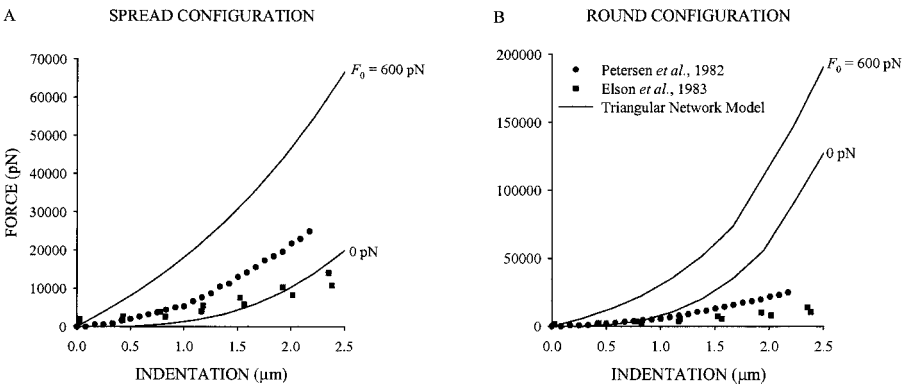

FIGURE 5 Triangular cable network model response to cell poking deformation. Comparison of the predicted indentation u versus force W relationships (*lines*) and measured data (*symbols*) from Petersen et al. (1982) and Elson et al. (1983) for the (*A*) spread and (*B*) round model configurations with $F_0 = 0$ and 600 pN.

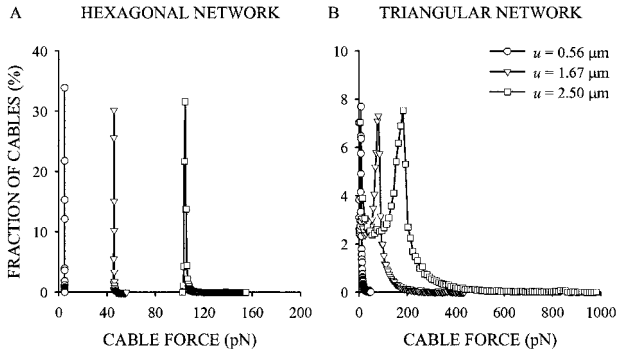

FIGURE 6 (*A*) Histograms of cable forces for the (*A*) hexagonal and (*B*) triangular network models in the spread model configuration for indentations $u = 0.56$, 1.67, and 2.5 μm and $F_0 = 0$ pN. Each histogram consists of 100 evenly spaced bins between the minimum and maximum cable force at each u.

response are not the primary determinants of the cell response. Thus, kinematics of the planar network of actin filaments may not be the primary determinant of the cell response to MTC. However, the observed decrease in deformability with increasing CSK forces was captured by the model suggesting that F_0 may contribute to the cell response.

Magnetic bead microrheometry

In both the hexagonal (Fig. 8) and triangular (*not shown*) networks in the round and spread (*not shown*) configurations, $\mathcal{F}$ increased with increasing δ which is consistent with MBM measurements on adherent fibroblast (Bausch et al., 1998) and endothelial cells (Bausch et al., 2001). The dependence of $\mathcal{F}$ on δ is nearly linear, which is consistent with the measured data. For a given δ, $\mathcal{F}$ increased with increasing with F_0. This observation agrees with the decrease in endothelial cell deformability after pharmacological activation (Bausch et al., 2001). The quantitative predictions

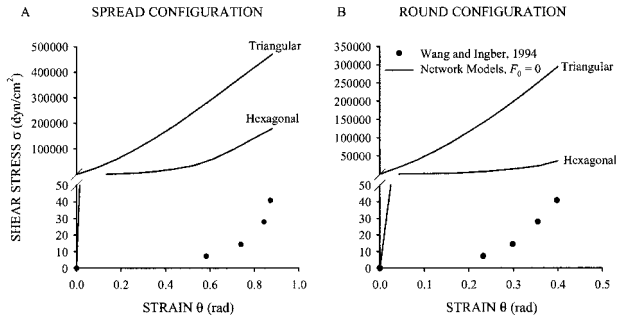

FIGURE 7 Hexagonal and triangular cable network models response to cell magnetic twisting cytometry deformation. Comparison of the predicted shear stress σ versus strain θ relationships (*lines*) and measured data (*symbols*) from Wang and Ingber (1994) for the (*A*) spread and (*B*) round model configurations with $F_0 = 0$ only. The ticks are unevenly spaced before and after the break in the ordinate to display both the measured data and predicted values.

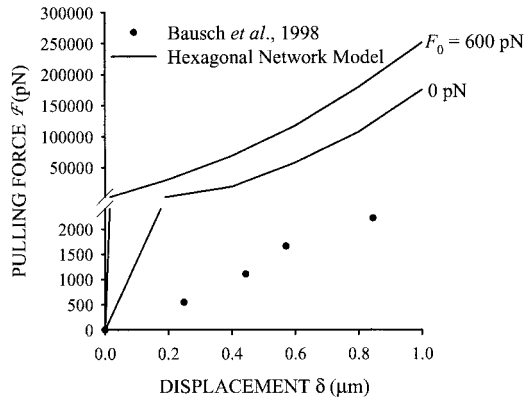

FIGURE 8 Hexagonal cable network model response to magnetic bead microrheometry deformation. Comparison of the predicted pulling force $\mathcal{F}$ versus displacement δ relationships (*lines*) and measured data (*symbols*) from Bausch et al. (1998) for the round model configuration with $F_0 = 0$ and 600 pN. The ticks are unevenly spaced before and after the break in the ordinate to display both the measured data and predicted values.

of $\mathcal{F}$ from all models exceed the measured values by several orders of magnitude (Fig. 8).

DISCUSSION

The model presented herein is derived from a conceptual model of the adherent cell CSK in which the mechanical response is determined by prestress and kinematics of elastic cables. This class of structures has proven particularly insightful in elucidating mechanics of the CSK for various cells (Hansen et al., 1996; Stamenović et al., 1996; Coughlin and Stamenović, 1997; Hansen et al., 1997; Coughlin and Stamenović, 1998; Discher et al., 1998; Stamenović and Coughlin, 1999; Stamenović and Coughlin, 2000). In particular, cable network models of the spectrin CSK of suspended red blood cells predict the response to micropipette aspiration. In this study, network models were applied to the mechanics of the adherent cell CSK. The features of the models were based on published ultrastructural observations and mechanical measurements from both living cells and individual CSK filaments. The CSK elasticity was attributed solely to a dense network of interconnected actin filaments. This view is consistent with measurements on several adherent cell types showing that actin filaments determine the cell mechanical response and ultrastructural observations of the adherent cell CSK showing a preponderance of actin filaments where these cells are probed. The representation of individual actin filaments in the model as stiff, linear elastic cables follows from their observed tensile response (Kojima et al., 1994) and a detailed analysis of their mechanical properties (Gittes et al., 1993). The many interactions observed between interconnected filaments in the CSK (whether chemical, stearic, or other) were represented in the model by frictionless pin-joints, and the resulting network porosity and filament segment length was

$\sim 10^1$–10^2 nm. Many actin cross-linking proteins have been identified in a variety of adherent cells, and ultrastructural observations confirm the appearance of a dense, interconnected network permeating the cell cytoplasm. Fixed pin-joints in the model represented local regions of firm adhesion between an adherent cell and rigid substrate. The model was deformed to mimic CSK deformation imposed during CP, MTC, and MBM measurements on living adherent cells.

The model best captured the qualitative and quantitative features of the adherent cell mechanical response to CP deformation. The model exhibits strain hardening and decreased deformability with increasing F_0. Both of these findings are consistent with observations from CP measurements on adherent fibroblast cells (Petersen et al., 1982; Elson et al., 1983; Cai et al., 1998). Moreover, the measured CP data fall between the predicted upper and lower bounds of W. Taken together, these findings support the assertion that the mechanisms determining model deformability are present within living adherent cells. That is, the prestressed peripheral actin CSK is a key determinant of adherent fibroblast cell deformability and filament kinematics is responsible for the nonlinear mechanical response. The model revealed that externally applied forces are transmitted throughout the actin CSK, with peripheral filaments contributing to resistance to local deformation. This differs from continuum based predictions where the deformation rapidly decays in the radial direction from the point of load application (Sokolnikoff, 1946). The model was unable to quantitatively predict the response of adherent cells to MTC or MBM. However, some qualitative features of the cell response were captured by the model. Thus, the cable network has limited applicability in describing the mechanics of adherent cells. Despite those limitations, filament tension was identified as a key determinant in the cell response to MTC and MBM.

A surprising aspect of this analysis is the dichotomy in the ability of the model to qualitatively and quantitatively capture the CP response while failing to predict many facets of the MTC or MBM response. Many of the important differences in the measurement techniques that may explain these discrepancies are accounted for in the model, e.g., probe size, mode of deformation, extent of deformation. However, some others are not. A feature common to MTC and MBM that is not found in CP is the probable recruitment of CSK and associated proteins to the probe. In the case of CP, forces to resist punch indentation emanate from the cortical CSK which is accurately modeled by a planar network. On the other hand, in the case of MTC and MBM, accumulation of focal adhesion proteins may bring additional CSK elements (e.g., more filaments) or structures (e.g., stress fibers) to the probe. The ensuing deformation is resisted by both the cortical CSK and the recruited CSK components. This additional structure may introduce new mechanisms or components that contribute to cell deformability but are not included in the models. For example, forces may be transmitted deeper into the cytoplasm where the CSK network is more disorganized and heterogeneous than the subcortical CSK. Also, beads thought to only rotate in MTC measurements may also translate (Fabry et al., 2001), and the translating beads in MBM measurements may also rotate. Including these additional motions in the models would likely lower the predicted moments and pulling forces in MTC and MBM measurements, respectively, but not enough to account for the several orders of magnitude. In addition to in-plane twisting as a model for MTC reported here, twisting of the beads out of the plane of the network was also examined. Twisting out of the plane of the network corresponds more closely to the actual motion of the beads in MTC measurements. The bound pin-joints were rotated as a rigid body through an angle θ about an axis in the plane of the network and perpendicular to an axis of mirror symmetry. The equilibrium positions of the free pin-joints were determined from Eq. 4 as described. The shear stress σ was computed as before. The hexagonal model in the round configuration predicts the nonlinear increase in σ with increasing θ observed in MTC measurements, and, for a given θ, the model predicts increasing σ with increasing F_0 (Fig. 9). The quantitative predictions of σ are one-half to one-third of the predicted values of the corresponding model for in-plane twisting, however, they still far exceed the measured values.

Comparing the model response at various F_0 to the initial cell response to cell poking ($u < 0.5$ μm) gives an estimate to the initial tension in individual actin filaments in living fibroblast cells. Several data points were extracted from the initial indentation of adherent fibroblast cells (Petersen et al., 1982) and compared to the predictions at those u for the hexagonal network in the spread configuration. The minimum least squares difference between the measured

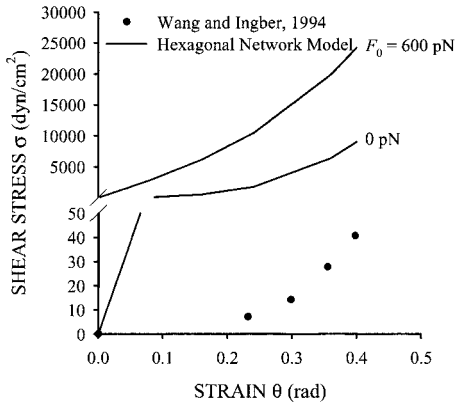

FIGURE 9 Hexagonal cable network model response to cell magnetic twisting cytometry deformation where the bead rotation is out of the plane of the network. Comparison of the predicted shear stress σ versus strain θ relationships (*lines*) and measured data (*symbols*) from Wang and Ingber (1994) for the round model configuration with $F_0 = 0$ and 600 pN. The ticks are unevenly spaced before and after the break in the ordinate to display both the measured data and predicted values.

data and the model prediction was found for $F_0 \approx 158$ pN. This suggests the actin filament tension in the peripheral CSK in adherent fibroblast cells is ~158 pN.

To formulate computationally tractable models that still retain the major features of the CSK mechanical response, a number of factors known to contribute to cell deformability were not included in the model formulations. The models do not include dissipative phenomena, such as viscous losses. Measurements of various cell types and measurement techniques exhibit hysteresis or loss mechanisms (Petersen et al., 1982; Elson et al., 1983; Shroff et al., 1995; Bausch et al., 1998; Maksym et al., 2000). Also, the models do not include mechanical contributions from other structures such as membranes, microtubules, intermediate filaments, or the nucleus. Several studies indicate the contribution of membrane forces to resisting deformation imposed during mechanical measurements accounts for ~30% (Wang et al., 1993) or substantially less (Petersen et al., 1981) of the cell resistance to deformation. However, the model does not include bending resistance to deformation of the membrane cortex (i.e., the membrane and peripheral CSK) which is a key mechanism in micropipette aspiration experiments of suspended neutrophils (Zhelev et al., 1994) and appears implicitly in network models of the spectrin network of suspended erythrocytes (Discher et al., 1998). Because the membrane cortex of adherent cells is a curved and bendable structure, local curvature in the region of the probes may explain the quantitative disparity in the model predictions. Smaller probes may induce more bending deformation than larger probes. Interestingly, the model successfully predicted the fibroblast cell response to CP, which features a smaller probe than either MTC or MBM. In the case of MTC measurements, the apparent endothelial cell resistance to deformation decreased by ~30% when probed with ~25% smaller diameter beads (1.4 μm vs. 5.5 μm) (Wang and Ingber, 1994) suggesting other mechanisms may be more prevalent than bending of the cell cortex. The hexagonal model deformed to mimic MTC predicts an increased resistance to deformation by ~50% with 1.4 μm-diameter beads (Coughlin, 2000). No data is available from measurements with different probe sizes using CP or MBM. Loss of microtubule integrity is less damaging to cell deformability than loss of actin filament integrity in adherent fibroblast cells (Petersen et al., 1981). In fact, measurements from fibroblast cells using AFM show regions rich in microtubules correspond to soft regions of the cell surface. The nucleus influences measures of cellular deformability (Petersen et al., 1982; Elson et al., 1983). For small deformations, the influence of the nucleus may be minimal because the initial resistance to CP deformation is nearly constant both over and away from the nucleus (Elson et al., 1983). Additionally, dynamics of polymer filaments were ignored in the models. It is known that the CSK undergoes perpetual turnover and rearrangement mediated by several mechanisms (e.g., filament polymerization, depolymerization, severing). Also, based on the results of this analysis, actin filaments in the cortical CSK must support a prestress of the order 10^2 pN without breaking for the duration of the cell poking measurements. In studies measuring the actin filament yield force, the duration the filament was held under tension was not given particular attention. However, actin filaments were reported to support a tensile force near the yield force for more than 10 min (Kishino and Yanagida, 1988). A latter study showed measurements made over shorter time scales of ~20 s (Tsuda et al., 1996). Both times are longer than the indentation time of 2.5 s in cell poking measurements. Thus, it might not be unreasonable to assume that actin filaments behave like elastic cables on those time scales.

SUMMARY

Interconnected elastic cable networks were used to investigate the adherent cell mechanics. The tensed cortical actin network was identified as the main intracellular structure that provides resistance to CP deformation. The failure of the model to fully describe the cell response to MTC and MBM measurements suggest that the model is incomplete. Despite those shortcomings, the model provided insight into mechanisms by which the cortical CSK provides shape stability to the cell. Filament tension provides the mechanical integrity that determines cell deformability. Filament kinematics is responsible for the nonlinear CP response. Filament tension is a key determinant in the cell response to MTC and MBM.

This study was supported by U. S. Public Health Service (HL43024) and National Heart, Lung and Blood Institute (HL33009).

REFERENCES

Amos, L. A., and W. B. Amos. 1991. Molecules of the Cytoskeleton. The Guilford Press, New York.

Bausch, A. R., U. Hellerer, M. Essler, M. Aepfelbacher, and E. Sackmann. 2001. Rapid stiffening of integrin receptor-actin linkages in endothelial cells stimulated with thrombin: a magnetic bead microrheology study. *Biophys. J.* 80:2649–2657.

Bausch, A. R., F. Ziemann, A. A. Boulbitch, K. Jacobson, and E. Sackmann. 1998. Local measurements of viscoelastic parameters of adherent cell surfaces by magnetic bead microrheometry. *Biophys. J.* 75:2038–2049.

Cai, S., L. Pestic-Dragovich, M. E. O'Donnell, N. Wang, D. E. Ingber, E. Elson, and P. De Lanerolle. 1998. Regulation of cytoskeletal mechanics and cell growth by myosin light chain phosphorylation. *Am. J. Physiol.* 275:C1349–C1356.

Caille, N., Y. Tardy, and J. J. Meister. 1998. Assessment of strain field in endothelial cells subjected to uniaxial deformation of their substrate. *Ann. Biomed. Eng.* 26:409–416.

Chen, C. S., M. Mrksich, S. Huang, G. M. Whitesides, and D. E. Ingber. 1997. Geometric control of cell life and death. *Science*. 276:1425–1428.

Chicurel, M. E., C. S. Chen, and D. E. Ingber. 1998. Cellular control lies in the balance of forces. *Curr. Opin. Cell Biol.* 10:232–239.

Coughlin, M. F. 2000. The Microstructural Basis of Cellular Deformability. Dissertation. Department of Biomedical Engineering, Boston University, Boston.

Coughlin, M. F., and D. Stamenović. 1997. A tensegrity structure with buckling compression elements: applications to cell mechanics. *J. Appl. Mech.* 64:480–486.

Coughlin, M. F., and D. Stamenović. 1998. A tensegrity model of the cytoskeleton in spread and round cells. *J. Biomech. Eng.* 120:770–777.

Discher, D. E., D. H. Boal, and S. K. Boey. 1998. Simulations of the erythrocyte cytoskeleton at large deformation. II. Micropipette aspiration. *Biophys. J.* 75:1584–1597.

Elson, E. L. 1988. Cellular mechanics as an indicator of cytoskeletal structure and function. *In* Annual Review of Biophysics and Biophysical Chemistry. D. M. Engelman, C. R. Cantor, and T. D. Pollard, editors. Annual Reviews Inc., Palo Alto. 397–430.

Elson, E. L., B. B. Daily, W. B. McConnaughey, C. Pasternak, and N. O. Petersen. 1983. Measurement of forces which determine the shapes of adherent cells in culture. *In* Frontiers in Biochemical and Biophysical Studies of Proteins and Membranes. T.-Y. Liu, S. Sakakibara, A. N. Schechter, K. Yagi, K. Yajima, and K. T. Yasunobu, editors. Elsevier Science Publishing Co., Inc., New York. 399–411.

Fabry, B., G. N. Maksym, J. P. Butler, M. Glogauer, D. Navajas, and J. J. Fredberg. 2001. Scaling the microrheology of living cells. *Phys. Rev. Lett.* 87:148102.

Folkman, J., and A. Mascona. 1978. Role of cell shape in growth control. *Nature.* 273:345–349.

Gerald, C. F., and P. O. Wheatley. 1989. Applied Numerical Analysis. Addison-Wesley Publishing Company, Inc., Reading.

Gittes, F., B. Mickey, J. Nettleton, and J. Howard. 1993. Flexural rigidity of microtubules and actin filaments measured from thermal fluctuations in shape. *J. Cell Biol.* 120:923–934.

Hansen, J. C., R. Skalak, S. Chien, and A. Hoger. 1996. An elastic network model based on the structure of the red blood cell membrane skeleton. *Biophys. J.* 70:146–166.

Hansen, J. C., R. Skalak, S. Chien, and A. Hoger. 1997. Influence of network topology on the elasticity of the red blood cell membrane skeleton. *Biophys. J.* 72:2369–2381.

Hubmayr, R. D., S. A. Shore, J. J. Fredberg, E. Planus, R. A. Panettieri, W. Moller, J. Heyder, and N. Wang. 1996. Pharmacological activation changes stiffness of cultured human airway smooth muscle cells. *Am. J. Physiol.* 271:C1660–C1668.

Janmey, P. A. 1996. Coping with cellular stress: the mechanical resistance of porous protein networks. *Biophys. J.* 71:3–5.

Janmey, P. A. 1998. The cytoskeleton and cell signaling: component localization and mechanical coupling. *Physiol. Rev.* 78:763–781.

Kishino, A., and T. Yanagida. 1988. Force measurements by micromanipulation of a single actin filament by glass needles. *Nature.* 334:74–76.

Kojima, H., A. Ishijima, and T. Yanagida. 1994. Direct measurement of stiffness of single actin filaments with and without tropomyosin by *in vitro* nanomanipulation. *Proc. Natl. Acad. Sci. USA.* 91:12962–12966.

Luby-Phelps, K., D. L. Taylor, and F. Lanni. 1986. Probing the structure of cytoplasm. *J. Cell Biol.* 102:2015–2022.

Maksym, G. N., B. Fabry, J. P. Butler, D. Navajas, D. J. Tschumperlin, J. D. Laporte, and J. J. Fredberg. 2000. Mechanical properties of cultured human airway smooth muscle cells from 0.05 to 0.4 Hz. *J. Appl. Physiol.* 89:1619–1632.

McConnaughey, W. B., and N. O. Petersen. 1980. Cell poker: an apparatus for stress-strain measurements on living cells. *Rev. Sci. Instrum.* 51: 575–580.

Petersen, N. O., W. B. McConnaughey, and E. L. Elson. 1981. Investigations of structural determinants of cell shape. *Comm. Molec. Cell. Biophys.* 1:135–147.

Petersen, N. O., W. B. McConnaughey, and E. L. Elson. 1982. Dependence of locally measured cellular deformability on position on the cell, temperature, and cytochalasin B. *Proc. Natl. Acad. Sci. USA.* 79:5327–5331.

Pourati, J., A. Maniotis, D. Spiegel, J. L. Schaffer, J. P. Butler, J. J. Fredberg, D. E. Ingber, D. Stamenović, and N. Wang. 1998. Is cytoskeletal tension a major determinant of cell deformability in adherent endothelial cells? *Am. J. Physiol.* 274:C1283–C1289.

Satcher, R., C. F. Dewey, Jr., and J. H. Hartwig. 1997. Mechanical remodeling of the endothelial surface and actin cytoskeleton induced by fluid flow. *Microcirculation.* 4:439–453.

Shroff, S. G., D. R. Saner, and R. Lal. 1995. Dynamic micromechanical properties of cultured rat atrial myocytes measured by atomic force microscopy. *Am. J. Physiol.* 269:C286–C292.

Singhvi, R., A. Kumar, G. P. Lopez, G. N. Stephanopoulos, D. I. C. Wang, G. M. Whitesides, and D. E. Ingber. 1994. Engineering cell shape and function. *Science.* 264:696–698.

Sokolnikoff, I. S. 1946. Mathematical Theory of Elasticity. Krieger Publishing Company, Malabar.

Stamenović, D., and M. F. Coughlin. 2000. A quantitative model of cellular elasticity based on tensegrity. *J. Biomech. Eng.* 122:39–43.

Stamenović, D., and M. F. Coughlin. 1999b. The role of prestress and architecture of the cytoskeleton and deformability of cytoskeletal filaments in mechanics of adherent cells: a quantitative study. *J. Theor. Biol.* 201:63–74.

Stamenović, D., J. J. Fredberg, N. Wang, J. P. Butler, and D. E. Ingber. 1996. A microstructural approach to cytoskeletal mechanics based on tensegrity. *J. Theor. Biol.* 181:125–136.

Stamenović, D., and N. Wang. 2000. Cellular responses to mechanical stress: engineering approaches to cytoskeletal mechanics. *J. Appl. Physiol.* 89:2085–2090.

Tsuda, Y., H. Yasutake, A. Ishijima, and T. Yanagida. 1996. Torsional rigidity of single actin filaments and actin-actin bond breaking force under torsion measured directly by *in vitro* micromanipulation. *Proc. Natl. Acad. Sci. USA.* 93:12937–12942.

Wang, N., J. P. Butler, and D. E. Ingber. 1993. Mechanotransduction across the cell surface and through the cytoskeleton. *Science.* 260:1124–1127.

Wang, N., and D. E. Ingber. 1994. Control of cytoskeletal mechanics by extracellular matrix, cell shape, and mechanical tension. *Biophys. J.* 66:2181–2189.

Zahalak, G. I., W. B. McConnaughey, and E. L. Elson. 1990. Determination of cellular mechanical properties by cell poking, with an application to leukocytes. *J. Biomech. Eng.* 112:283–294.

Zhelev, D. V., D. Needham, and R. M. Hochmuth. 1994. Role of the membrane cortex in neutrophil deformation in small pipettes. *Biophys. J.* 67:696–705.